

## Flow Categorization in Supersonic Flows with Large Roughness Heights

H. van Pelt<sup>1</sup>, B.W. van Oudheusden<sup>1</sup>, F.F.J. Schrijer<sup>1</sup>, L.J. Souverein<sup>2</sup> and K. Seeliger<sup>2</sup>

<sup>1</sup>Department of Aerodynamics  
Delft University of Technology, Delft, The Netherlands

<sup>2</sup>TP22 - System Analysis & Modelling  
Airbus Defence & Space, Munich, Germany

### Abstract

In the present research the flow over large roughness elements, representative of a rocket nozzle inner contour, is investigated. From the rocket nozzle inner surface roughness, three simplified roughness shapes were defined and tested: a forward facing step, a cavity, and a forward facing step plus cavity. The geometries vary in height from 6 to 46 percent of the boundary layer thickness. The flow over these roughness elements is studied at a free stream Mach number of 2. This was done numerically by means of RANS simulations and experimentally by means of Schlieren and PIV. For these geometries it was found that three flow classes can be distinguished. For large roughness heights, with a large length to depth ratio, the flow disruptions center around the steps, while the sections between the elements show flat-plate flow. Drag and heat transfer show large increases for these elements. At smaller roughness heights a smoother behavior of the flow can be seen which more resembles boundary layer behavior. For cases where the length to depth ratio of the elements becomes small, a third flow class can be defined. Here the flow is separated between the roughness elements, and the gap from element top to element top is bridged by a shear layer. It was observed that a boundary layer was formed on top of the elements. Based on these observations, a classification system is proposed which divides the roughness in different categories, for each of which it is recommended to use a separate modelling approach.

### Introduction

To evaluate the thermal loading of a rocket nozzle, a good predictive capability of the heat transfer on the gas side is mandatory. For a smooth wall multiple design formulations are available to calculate the heat transfer, see White [5]. If the surface is rough the heating is likely to be different from the smooth case. The interest of the current research lies in the regime of large roughness heights (relative to the boundary layer thickness) since this is not well covered in literature. Jimenez [1] is one of the few sources that describes flows over larger roughnesses. In practice these rough wall geometries can have various forms and shapes. They can range from the distributed wall texture roughness, to discrete roughness elements. Material roughness has been extensively researched. It was shown by Nikuradse [3] that the turbulent boundary layer flow on a rough surface can be described by adapting the standard law of the wall. In this study, however, we consider discrete wall patterns that are designed to represent the surface irregularities on the inside of the baseline rocket nozzle due to the employed manufacturing technique. We will investigate the effects of such surface irregularities on the flow, focusing in particular on the size of these roughness profiles. The final goal is to find a model that can explain the observed effects. Different physical behavior has been observed in different configurations, and therefore a system will be proposed which classifies the roughness into categories with the same behavior. The investigation was carried out using a combined computational and experimental ap-

proach. First a CFD study has been performed on these geometries. These simulations were made for a turbulent flow over an adiabatic, heated and cooled wall. The non-adiabatic wall simulations, were run with a wall temperature of 0.5 and 1.5 times the adiabatic wall temperature, i.e., 137.5 K and 412.5 K, respectively. In the experiments the flow was visualized using Schlieren. Particle Image Velocimetry (PIV) was subsequently used to measure the velocity in the flow field.

### Rough geometries

To investigate the effect of element geometry on the wall shear and heat transfer, multiple geometries have been defined. These are variations on the baseline nozzle geometry. For optical access to the geometries in the experiments they have been implemented as spanwise two-dimensional shapes in a nominal flat-plate configuration. Fig. 1 A shows several elements of the baseline nozzle shape extrapolated to a flat plate with the free-stream from left to right.

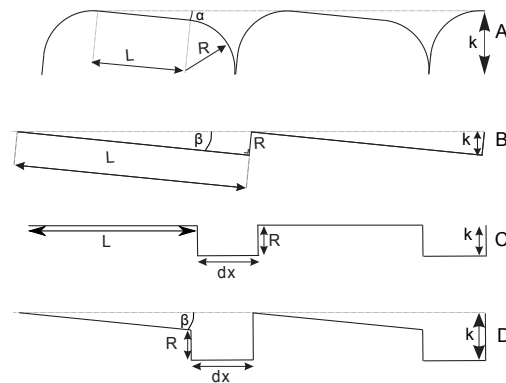


Figure 1: Roughness shape definitions

The flow is assumed to remain predominantly attached over the inclined section of length  $L$ , but separates in front of the next element. Therefore a cavity type flow, and a forward facing step flow will likely occur. Therefore the simplified geometries B, C and D will be considered alongside baseline geometry A. Geometry B is a forward facing step with a length  $L$  and a height  $R$ . Geometry C is a cavity. The cavity length ( $dx$ ) is 1.71 mm. Geometry D is a combination of a cavity and a forward facing step. The total horizontal length of element B and D is the same. This last geometry, relative to geometries B and C has given the opportunity to determine which of the two features (forward facing step, cavity) is the dominant one. The complete test matrix can be seen in Table 1.

Model	Shape	L/R	R (mm)	$k^+$
Flat plate	Flat plate	-	0	0
L48R25	Fig. 1 B	19.8	2.45	1414
L33R17	Fig. 1 B	19.8	1.66	960
L16R08	Fig. 1 B	19.8	0.83	480
L06R03	Fig. 1 B	19.8	0.33	190
Cavity	Fig. 1 C	19.8	1.66	960
L33R17C	Fig. 1 D	19.8	1.66	960
Full Geometry	Fig. 1 A	19.8	1.66	960
L10R17	Fig. 1 B	6.09	1.66	960
L06R17	Fig. 1 B	3.3	1.66	960

Table 1: Test Matrix

Table 1 shows the model name, its shape, the L/R ratio and the size of the roughness geometry in metric units and in wall units ( $k^+$ ). The absolute size of the roughness elements has been based on the undisturbed boundary layer characteristics and the baseline rocket nozzle geometry. The flat plate test case will be used as a reference. The influence of step height is investigated with the cases L48R25 till L06R03. "Cavity", "L33R17C" and "Full geometry" are included to investigate differences in shape. In the L10R17 and L06R17 geometries the height has been kept the same while the length has been reduced resulting in an increase in the spatial frequency of the roughness elements. The L48R25 geometry height is half of the undisturbed boundary layer thickness. The L33R17 geometry height is the size of the log-law of the undisturbed boundary layer. The L16R08 geometry is half of the L33R17 geometry. The L06R03 geometry is  $k^+$  similar to a representative point inside the baseline rocket nozzle. The L/R ratios for the L48R25 to L06R03 geometries are constant. The sizing of the rest of the geometries has been based on these geometries.

### Test Setup

The roughness geometries were investigated for a Mach 2 flow. To generated these condition in the supersonic wind tunnel, solid nozzle blocks are used which expand the flow from the throat to the test section. Since the roughness geometries cannot be incorporated into the wall itself, plates have been made which have the geometries fabricated into them. These plates were kept in place by a front and back insert. For the CFD investigations a clean inflow was deemed important, therefore the geometries were incorporated directly into the wall for the simulations.

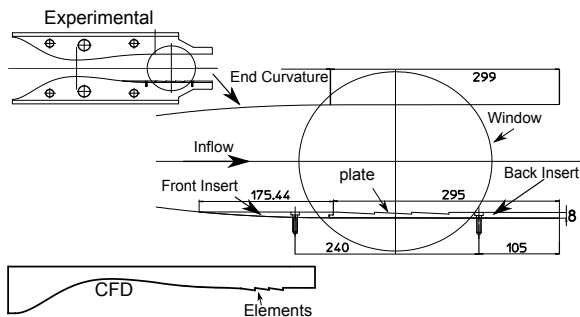


Figure 2: Test Environment

Figure 2 shows the test section and the geometries, the CFD elements are not in proportion. The inflow is at the left hand side. A nozzle geometry can be seen including the front insert, plate and back insert.

### CFD

In view of the (near) symmetry of the wind tunnel configuration, the numerical simulation was carried out on a half domain to save computational cost. A symmetry condition was imposed at the outer boundary of the computational domain, corresponding to the wind tunnel center line. The roughness geometries have been incorporated into the wind tunnel the wall for the CFD simulations, and not into plates. One reference simulation has also been made of the exact experimental geometry (including inserts) to investigate their influence. With the CFX solver, RANS simulations have been performed with an SST turbulence model. The SST model was used as it has been shown to be an adequate turbulence model for calculating wall-bounded flows involving separation, see Menter [2].

### Experimental Investigation

Two experimental techniques have been employed: Schlieren and particle image velocimetry (PIV). For the Schlieren set-up a standard Z-type black and white Schlieren system has been employed. For the PIV investigation 2D measurements have been made in the free stream wall normal plane with a Nd:YAG laser in combination with DEHS particles as seeding. The processing of the PIV images has been done with the software DaVis from Lavisision, in which the main routine is an iterative window deformation method with Gaussian weighing. Although more extensive PIV measurements have been performed, the present paper only contains PIV data for validation of the incoming boundary layer. The corresponding boundary layer properties are given in Table 2.

Data	Value	Data	Value
$\delta$ (mm)	5.18	$P_0$ (bar)	3.2
$\theta$ (mm)	0.42	$T_0$ (K)	290
$\delta^*$ (mm)	1.18	$C_f$ (-)	$1.94e-3$
$M_e$ (-)	2.04	$u_\tau$ (m/s)	20.84

Table 2: Data incoming boundary layer.

### Validation

A comparison between the experimental and numerical flat plate undisturbed boundary layer data was made for validation purposes. The experimental data was compared with the CFD solution (without inserts), and the CFD reference solution (solution including inserts).

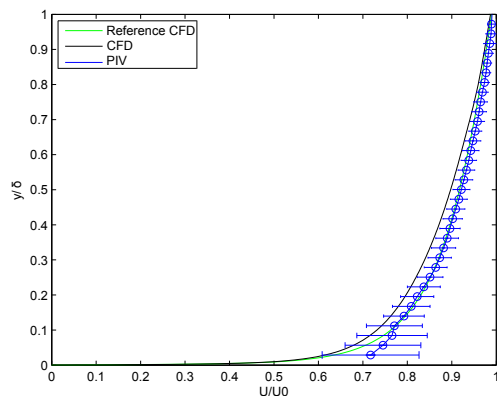


Figure 3: Velocity profiles at start test section

Figure 3 shows all the velocity profiles for the start of measurement section (at 3% of total test section length). The three lines

show the experimental PIV results (dark blue), the reference CFD (green) and the CFD solution (black). The error bars show the deviation with respect to the RMS of the velocity data. The height has been normalized by the boundary layer thickness, and the velocity has been normalized by the free-stream velocity. The reference CFD simulation shows good agreement with the experimental results. The mismatch for the first 3 data points is probably due to interrogation windows overlapping with the wall. The data from the CFD solution shows a discrepancy with that of the PIV data. This is due to the front insert, the influence on the flow due to this insert is still visible at the inflow of the test section. More downstream better matches have been found between the CFD solution and PIV results, see van Pelt [4].

## Results

Figures 4 and 5 show drag coefficient values and the order of magnitude differences for the heat transfer rate determined from the numerical flow simulations.

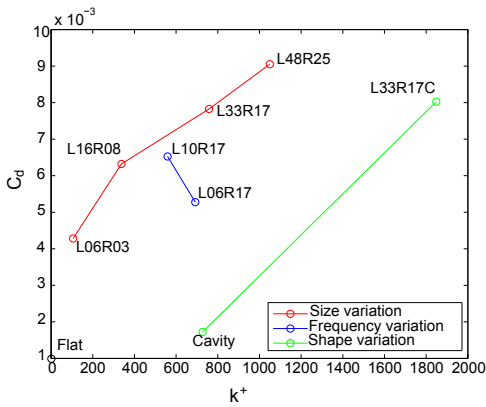


Figure 4: Drag coefficient

Figure 4 shows the drag coefficients for all the geometries. The three different lines illustrate the effects of variation in size (red), variation in frequency (blue), and the variation in shape (green). The red curve shows a non-linear increase in drag coefficient with increasing roughness height. The cavity shows an increase in drag with respect to the flat plate. The frequency variation shows a larger drag for a larger length. The drag coefficient of the L33R17 and L33R17C geometries are similar, while the cavity has a much smaller drag than the L33R17 geometry for the same roughness height. Therefore we can conclude that the step is the main source of drag, and not the cavity.

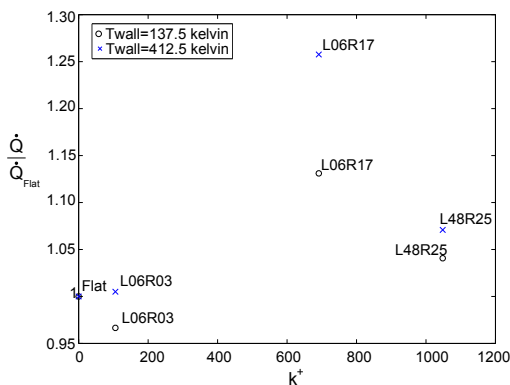


Figure 5: Normalized total heat flux

Figure 5 shows the heat transfer rate normalized by the flat plate value. It can be seen that the L06R03 and L48R25 cases are within a 10% range with respect to the flat plate case. The L06R17 case shows a larger increase. The L06R03 geometry has a small layer of separated flow inside the elements, which acts as an insulator, therefore the cooled heat transfer is lower than the flat plate value. For the heated case the boundary layer changes, therefore the heating in the first part of the elements is increased leading to a larger than flat plate heating.

A starting point for modelling is the determination if the flow can be modeled as a standard boundary layer flow, or as a flow where the elements themselves have to be modelled (element flow). Figure 6 shows the Schlieren image (right), and CFD results of the density gradient in the y direction (left) for the L48R25, L06R03 and L06R17 geometries.

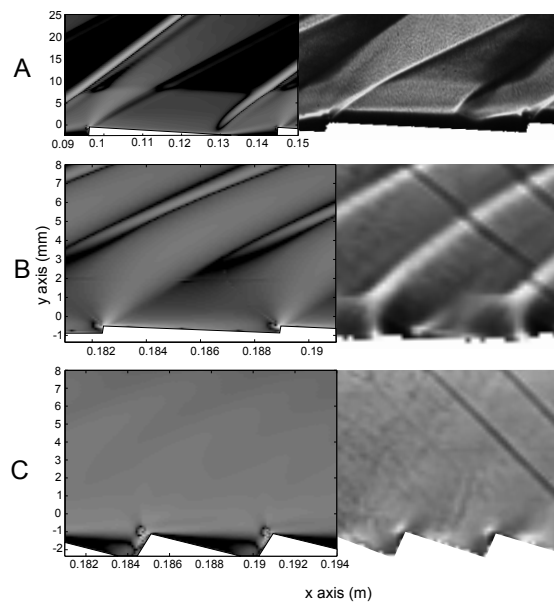


Figure 6: Flow field L48R25 (A), L06R03 (B), L06R17 (C) geometry

Figure 6 A shows an expansion wave directing the flow from the previous elements into the next element. There is then a section of flat plate flow, followed by a region of separated flow, accompanied by a separation shock. Since the elements are large with respect to the undisturbed boundary layer thickness ( $\frac{k}{\delta} = 0.46$ ) these flow features are predominant, causing significant pressure rises on the roughness faces.

In figure 6 B the flow field of the L06R03 geometry is shown. The elements are small with respect to the undisturbed boundary layer ( $\frac{k}{\delta} = 0.06$ ). The flow features are much smaller than for the L48R25 geometry. Therefore the flow much more resembles a continuous boundary layer flow.

The figure 6 C shows the flow field of the L06R17 geometry. These elements have a smaller wave length than in the other geometries. Because of that, the flow separates at the start of the element and the main flow continues over the elements. From the CFD Schlieren fields this can clearly be seen because of the large gradients inside the elements. For a quantitative discussion, the next section provides data on the boundary layer evaluation over the L33R17, L10R17 and L06R03 geometry.

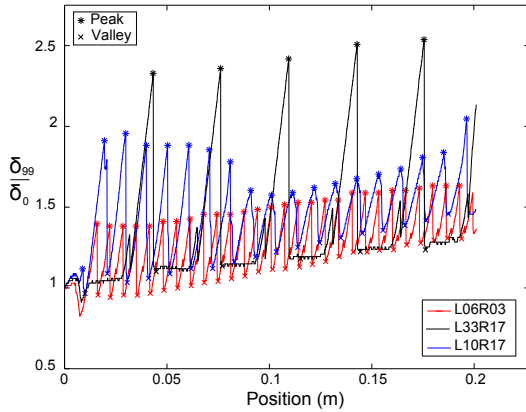


Figure 7: Normalized local boundary layer thickness: L33R17, L10R17 and L06R03 geometry

Figure 7 shows the local boundary layer thickness ( $\delta_{99}$ ) normalized by the undisturbed values ( $\delta_0$ ). The local boundary layer thickness has been measured from the wall of the roughness element. The areas of attached flow inside the roughness element are reflected by the semi-constant regions in the boundary layer thickness. After the separation point the boundary layer thickness measured from the wall is seen to increase. When the flow reaches a new element the flow attaches again, therefore there will be a sharp drop in the boundary layer thickness. The L48R25 and L16R08 cases shown the same type of behavior. The L10R17 and L06R03 geometries show no semi-constant regions, and therefore display no attached flow regions inside the elements. As was shown in van Pelt[4] the heat transfer is dominated by the attached flow regions. Therefore the L06R03 case shows a different flow field to that of the L33R17 and L48R25 geometries.

To characterize the distortion effect on the boundary layer a disturbance factor was defined based on the peak and valley values of the normalized boundary layer thickness and scaled with the roughness height, as:

$$D = \frac{P - V - k}{k} \quad (1)$$

Here the disturbance ( $D$ ) is related to the peak value of the boundary layer thickness ( $P$ ), the valley value of the boundary layer thickness distribution ( $V$ ) and the roughness height ( $k$ ).

Figure 8 shows the size of the disturbances. The cavity and L06R17 geometry evolve into a steady state boundary layer, because of small disturbance factors. The initial jump in the L06R17 data is attributed to numerical inaccuracies. The L10R17 geometry shown initially a larger disturbance factor, but with evolving boundary layer it's value declines. The L33R17 and L48R25 show a disturbance level of 4 and these two geometries also have a similar flow field. The L33R17C geometry shows a lower disturbance than the L33R17. This is because the flow separates in the cavity. Therefore the effective roughness height ( $k$ ) is similar, but the geometrical roughness height of the L33R17C geometry is higher, and therefore the disturbance is lower.

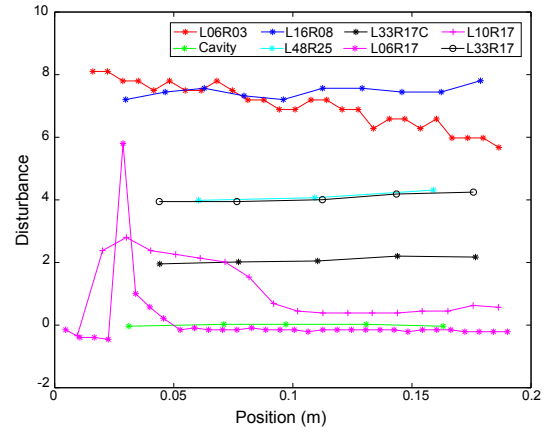


Figure 8: Axial disturbance factor distribution

The L16R08 and L06R03 have a large disturbance. For zero roughness height the disturbance goes to zero. Therefore the behavior of the L16R08 and L06R03 cases are interesting since it shows that for the roughness height going to zero the disturbances will first go up before it goes down to zero.

## Conclusion

In the current investigation three types of flows were identified. Based on the boundary layer characteristics there are roughness geometries which sustain a boundary layer, since the disturbances by the roughnesses are small. The L06R17, L10R17 and the cavity case display low disturbance levels because the boundary layer flows over the elements. For the large roughnesses, large disturbances can be seen, and strong flow features can also be observed. The L48R25, L33R17, L33R17C, L16R08 cases show large disturbances and strong flow features. Since the disturbances over the elements are large the flow cannot be modelled by a boundary layer model, the individual elements should be taken into account. The L06R03 geometry has a no attached flow inside the elements, but also no complete separation as for the L10R17 and L06R17 cases. Therefore the L06R03 geometry has a different boundary layer behavior compared to that of larger elements. Due to this different boundary layer behavior the heat transfer will behave differently. Therefore three flow classes can be defined based on their boundary layer and disturbance behavior. For these 3 classes different models for drag and heat transfer will have to be developed.

## References

- [1] Jimenez, J., Turbulent flows over rough walls, *Annual Review of Fluid Mechanics*, 2004.
- [2] Menter, F. R., Two-equation eddy-viscosity turbulence models for engineering applications, *AIAA*, 1994.
- [3] Nikuradse, J., Laws of flow in rough pipes, *NACA*, 1950.
- [4] van Pelt, H., *Flow modelling in supersonic flows with large roughness heights*, Master thesis, TU Delft, 2013.
- [5] White, F., *Viscous Fluid Flow, Third edition*, Mc-Graw Hill, 2006.